Construction of an ultrasensitive non-enzymatic sensor to investigate the dynamic process of superoxide anion release from living cells

Hongwei Wei, Tianyi Shang, Tiaodi Wu, Guoan Liu, Lan Ding, Xiuhui Liu

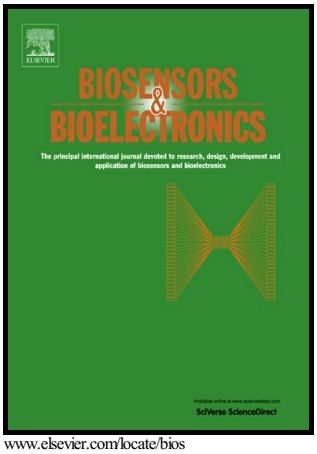

www.elsevier.com/locate/bios

PII: S0956-5663(17)30580-8
DOI: http://dx.doi.org/10.1016/j.bios.2017.08.046
Reference: BIOS9956

To appear in: *Biosensors and Bioelectronic*

Received date: 5 June 2017
Revised date: 18 August 2017
Accepted date: 21 August 2017

Cite this article as: Hongwei Wei, Tianyi Shang, Tiaodi Wu, Guoan Liu, Lan Ding and Xiuhui Liu, Construction of an ultrasensitive non-enzymatic sensor to investigate the dynamic process of superoxide anion release from living cells, *Biosensors and Bioelectronic,* http://dx.doi.org/10.1016/j.bios.2017.08.046

Construction of an ultrasensitive non-enzymatic sensor to investigate the dynamic process of superoxide anion release from living cells

Hongwei Wei, Tianyi Shang, Tiaodi Wu, Guoan Liu, Lan Ding, Xiuhui Liu*

Key Laboratory of Bioelectrochemistry & Environmental Analysis of Gansu Province, College of Chemistry & Chemical Engineering, Northwest Normal University, Lanzhou, 730070, China

* Corresponding author.

Xiuhui Liu， Tel.: +86 0931 7975276; E mail: liuxh@nwnu.edu.cn

Address: No. 967 Anning East Road, Lanzhou, Gansu, 730070. P.R.China

* Corresponding author. Tel.: +86 0931 7975276; fax: +86 0931 7971323. E mail: liuxh@nwnu.edu.cn

Abstract: In this work, a novel non-enzymatic superoxide anion ($O_2•^-$) sensor was constructed based on Ag nanoparticles (NPs) / poly (amidoamine) (PAMAM) dendrimers and used to investigate the dynamic process of $O_2•^-$ release from living cells. The AgNPs/PAMAM nanohybrids were characterized by transmission electron microscopy (TEM), cyclic voltammetry (CV) and electrochemical impedance spectroscopy (EIS). The fabricated electrode exhibited excellent catalytic activity toward the reaction of $O_2•^-$ with a super low detection limit (LOD) of 2.530×10^{-13} M (S/N=3) and wide linear range of 8 orders of magnitude. It could fulfill the requirement of real-time measurement $O_2•^-$ released from living cells. Furthermore, zymosan was chosen as the stimulant to induce $O_2•^-$ generation from cancer cells (rat adrenal medulla pheochromocytoma cell (PC12)). The electrochemical experiment results indicated that the levels of intracellular $O_2•^-$ depended on the amount of Zymosan. A large amount of $O_2•^-$ generated in the living cells by added heavy stimulant could damage cells seriously. More importantly, a vitro simulation experiment confirmed the role of superoxide dismutase (SOD) for the first time because it could maintain the $O_2•^-$ concentration at a normal physiological range. These findings are of great significance for evaluating the metabolic processes of $O_2•^-$ in the biological system, and this work has the tremendous potential application in clinical diagnostics to assess oxidative stress.

Keywords: Superoxide anion, Poly(amidoamine) dendrimers, Silver nanoparticles, Electrochemical biosensor, Living cell, Kinetic study.

1. Introduction

Superoxide anion ($O_2•^-$) is generated in various physiological oxidative processes in biological systems (Amatore et al, 2006; Wu et al, 2014). Basically, endogenous $O_2•^-$ came from two major sources: the mitochondrial respiratory chain and phagocytic NADPH oxidase. Activated NADPH oxidase in phagocytes assembled in membranes and reduced oxygen to superoxide (Hayyan et al, 2016a; Brand et al, 2004). On the other hand, $O_2•^-$ is also primary one of the reactive oxygen species (ROS). Exogenous sources of ROS are pollutants, smoke, drugs, radiation and other mediators (Prasad et al., 2017). Thus, $O_2•^-$ is a byproduct of respiration and a crucial component of the immune defense system (Su & Grives, 2010). Under normal

physiological conditions, $O_2^{\bullet -}$ plays an important role as a regulatory mediator in signaling processes (Amatore et al, 2008). Excessive accumulation of $O_2^{\bullet -}$ may cause damage to biological membranes, tissues, and organisms (Zhou et al., 2016). Hence, evaluating dynamic changes of $O_2^{\bullet -}$ concentration is of great significance in vitro and in vivo models. Up to date, many approaches have been used to measure $O_2^{\bullet -}$, such as spectrophotometry, electron spin resonance trapping, chemiluminescence and fluorometry (Haseloff et al., 1991; Kaji et al., 2009; Kalpana et al., 2009; Xie et al., 2008; Zweier et al., 1987). But, these methods are expensive and time-consuming. Compared with these techniques, electrochemical methods have received extensive attention owing to their intrinsic advantages such as simplicity, real-time detection directly, and possibility of in vivo detection (Ignatov et al., 2002). Especially, enzyme-based electrochemical biosensors (superoxide dismutase (SOD)) have always been the research highlights (Wu et al., 2014; Zhu et al., 2016). Unfortunately, the deeply buried redox centers of enzyme result in the slow electron transfer between enzyme and electrode. In addition, the enzyme-based biosensors suffer from relatively high cost, short lifetime, poor reproducibility and the critical operating situation (Dai et al., 2009; Wang et al., 2016). Therefore, it is a challenge to find an effective method monitoring kinetic process of $O_2^{\bullet -}$ release in biological system.

In recent years, nanomaterials have attracted much interest for their potential application in medicine and electrochemical fields. Especially, noble metal nanoparticles (NPs), such as AuNPs, PtNPs and AgNPs have become excellent substitutes for enzymes to catalyze the $O_2^{\bullet -}$(Cui et al., 2008; Li et al., 2012; Li et al., 2014; Li et al., 2013). Among the metal nanocatalysts, silver-based electrocatalytic materials have been widely used to modify electrodes due to their high electrocatalytic activity. Our group had constructed a variety of biosensors with AgNPs previously (Li et al., 2013; Liu et al., 2017b). These experiment results found that the electrocatalytic activity and stability of AgNPs were strongly dependent on the size, shape and distribution on the modified electrode (Liu et al., 2017b). Hence, it is very important to prepare the matrix for dispersed nanocatalysts highly.

Polyamidoamine (PAMAM) dendrimers are highly branched three-dimensional macromolecules with hydrophilic terminal functional groups ($–NH_2$) (An et al., 2012). Recently, they were applied to electrochemical fields due to high geometric symmetry, monodisperse, film-forming ability and chemical stability (Ning et al., 2014).

Moreover, PAMAM dendrimers could be immobilized on the electrode surfaces easily by polyvalent interactions such as surface coatings or cross-linking (Kavosi et al., 2014). Especially, study found that the fourth generation PAMAM (G4.0) dendrimers has spherical structure with diameter of approximately 4.5 nm and possesses 64 primary amine groups on the surface (Li et al., 2009). The interior cavities and surface functionalities offer multiple sites to load large amounts of metal nanoparticles. (Esfand & Tomalia, 2001; Tomalia, 2012; Wang et al., 2013). Thus, the presence of the PAMAM can avoid the aggregation of metal nanoparticles effectively. Up to now, some groups focused on utilizing PAMAM as the templates to synthesize monometallic, alloy, core/shell and bimetallic NPs catalysts (Hu et al., 2012; Lang et al., 2004; Scott et al., 2004). However, there is no report about electrodepositing metal NPs on PAMAM as nanocatalysts. Thus, we try to utilize PAMAM as the matrix for supporting AgNPs catalysts, and the nanohybrids show high catalytic activity.

In this work, a non-enzymatic $O_2^{\bullet -}$ sensor based on PAMAM and AgNPs was constructed and used to measure the $O_2^{\bullet -}$ released from living cells. The AgNPs/PAMAM/GCE exhibited outstanding performance towards $O_2^{\bullet -}$ with super wide linear range, very low detection limit and excellent reproducibility. More importantly, the presented sensor can be successfully used for monitoring the changes of $O_2^{\bullet -}$ levels from living cells and collecting kinetic information on cellular ROS release, which provides great help to understand the significance of superoxide dismutases (SOD) in biology and pathology.

2. Experimental section

2.1. Apparatus

The transmission electron microscopy (TEM) images were obtained from JEM-3010 transmission electron microscope (JEOL Co., Ltd., Japan). Electrochemical measurements were performed on a CHI660C electrochemical workstation (Austin, TX, USA) with conventional three-electrode system. A bare or modified glassy carbon electrode (GCE, d=3.0 mm) was employed as working electrode. A platinum electrode and a saturated calomel electrode (SCE) were served as the auxiliary and

reference electrode. All potentials given in this paper were referred to the SCE. Electrochemical impedance spectroscopy (EIS) experiments were performed on Multi-potentiostat (VMP2, Princeton Applied Research, USA). Ultraviolet-Visible spectroscope (UV–vis, EVOLUTION 220, Thermo Scientific) was used to detect the concentration of $O_2•^-$ obtained from the KO_2 stock solution. Before each electrochemical measurement, solutions were thoroughly deoxygenated by bubbling nitrogen through the solution for at least 20 min to remove dissolved oxygen.

2.2. Reagents

Ethylenediamine and methyl acrylate obtained from Tianjin No. 1 Chemical Reagent Factory (Tianjin, China) were used for the synthesis of PAMAM dendrimers of different generations. KO_2 was obtained from Aladdin Industrial Inc. DMSO was purchased from Beijing Chemical Works (Beijing, China). 18-crown-6 was bought from Energy Chemical (Shanghai Chemical Industries, Ltd.). 4 Å molecular sieve was obtained from Tianjin Kermel Chemical Industries, Ltd (Tianjin, China). Zymosan A and Superoxide dismutase (SOD) were bought from Sigma (USA). $AgNO_3$ and KNO_3 were purchased from Xi'an Chemical Reagent (Xi'an, China). PBS (pH 7.0) was prepared by mixing suitable amounts of 0.2 M NaH_2PO_4/Na_2HPO_4. Other chemicals were all of analytical grade, and the solutions were prepared by doubly distilled water.

2.3. Preparation of the $O_2•^-$ sensor

A glassy carbon electrode (GCE) was polished with 1.0, 0.3 and 0.05 μm alumina slurry to a mirror-like, respectively, followed by rinsing thoroughly with doubly distilled water. The electrode was successively sonicated in 1:1 nitric acid, acetone and doubly distilled water, and then allowed to dry at room temperature. Then 7 μL of PAMAM-G4.0 dendrimers aqueous solution (0.5 mg/mL) was dropped on the surface of GCE and dried in air, and the PAMAM/GCE was obtained. Next, the electrode was electrodeposited in the solution containing 1.0 mM $AgNO_3$ and 0.1 M KNO_3 for 180 s at 0 V to obtain AgNPs/PAMAM modified electrode.

2.4. Generation of superoxide anion

The chemical generation of $O_2•^-$ was performed by dissolving KO_2 in dimethyl

sulphoxide (DMSO) solution (containing 18-crown-6), and stored together with 4 Å molecular sieve. The solubility of KO_2 in DMSO can be increased by adding 18-crown-6. After sonicating the solution for 5 min, additional 4 Å molecular sieve was added to remove traces of H_2O. According to the molar absorptivity of $O_2•^-$ in DMSO (2006 M^{-1} cm^{-1} at 271 nm), the concentration of $O_2•^-$ could be estimated by a UV–Vis spectroscope (Hayyan et al., 2016).

2.5. Cell culture

PC12 (rat adrenal medulla pheochromocytoma) cells were obtained from Institute of Hematology, Chinese Academy of Medical Sciences. They were maintained in DMEM (high glucose, Gibco) medium supplemented with 10% heat-inactivated fetal calf serum (Evergreen, China), 100 U/mL penicillin (Sigma, USA), and 100 mg/mL streptomycin (Sigma, USA) at 37 °C with 5% CO_2 in a 95% humidified atmosphere.

2.6. Electrochemical detection of $O_2•^-$ released from cells

PC12 cells grown in 25 cm^2 cell culture flasks were seeded in a 6-well plate (1.5×10^5 cells per well) for 24 h for electrochemical experiments. Cell number was estimated by a cell counter. The media was removed and the cells were washed two times with phosphate-buffered saline, then 3 mL phosphate-buffered saline was added for real sample measurements. The amperometric detection of the release $O_2•^-$ from PC12 cells was performed using the AgNPs/PAMAM/GCE at −0.5 V (vs. SCE). When the current went to a stable level, zymosan was injected to the cells suspension, which can motivate cells generation of $O_2•^-$. The experiments were conducted in the water bath at 37 °C.

3. Results and discussion

3.1. Characterization of AgNPs/PAMAM/GC electrode

3.1.1. Morphological characterization and electrochemical behaviors of AgNPs/PAMAM nanohybrids

The morphology of the obtained materials was characterized with transmission electron microscope (TEM) images. As shown in Fig. 1A, AgNPs were

electrodeposited on the bare GCE surface with agglomeration obviously. But in Fig. 1B, as the GCE was covered uniformly with polyamidoamine (PAMAM) dendrimers film first and then AgNPs were electrodeposited on PAMAM-G4.0 composite, one can see that high density AgNPs were well separated from each other and uniformly distributed on the PAMAM matrix with the average diameter of 20 nm.

In order to further characterize the modified material, we did the electrochemical experiments as shown in Fig. 1C and D. In curve a of Fig. 1C, a cathodic peak at 0.326 V and a sharp anodic peak at 0.581 V appeared on the bare GCE, which were attributed to the redox peaks of 1.0 mM $AgNO_3$. When the PAMAM modified electrode was scanned in the same solution, the redox peak position did not change obviously in curve b, revealing that PAMAM composites could serve as matrix for the deposition of AgNPs. Fig. 1D showed CVs of AgNPs/GCE (curve a) and AgNPs/PAMAM/GCE (curve b) in N_2-saturated 0.2 M PBS (pH 7.0), respectively. A pair of peaks was also observed in each CV, which was ascribed to oxidation of Ag and reduction of Ag^+, proving the existence of AgNPs on the bare GCE and modified electrode, respectively. It is noticeable that the peak current of AgNPs/PAMAM/GCE (curve b) is much higher than that of the AgNPs/GCE (Fig. 1D curve a), suggesting great amount of AgNPs loaded on PAMAM/GCE. These phenomena indicated that PAMAM composites have a large surface and can be used as effective load matrix for the deposition of AgNPs on GCE.

Fig. 1

3.1.2. Electrochemical characterization of AgNPs/PAMAM/GCE

The electrocatalytic activities of the modified electrodes were studied using cyclic voltammetry (CV). Fig. 2A shows typical cyclic voltammograms of different electrodes in 5.0 mM $[Fe(CN)_6]^{3-/4-}$ and 0.1 M KNO_3. A pair of redox peaks was assigned to the redox of $[Fe(CN)_6]^{3-/4-}$. Compared with bare GCE (curve a), the anodic peak and cathodic peak of curve b increased in PAMAM/GCE, which further confirmed that the PAMAM could enhance the conductivity of the modified electrode. However, when AgNPs were electrodeposited on the PAMAM/GCE surface, the current value decreased obviously in curve c. The main reason, we think, may be ascribed to the quantum size effect of AgNPs. According to Kubo theory (Liu et al.,

2017b), the smaller the silver nanoparticle, the more obvious the quantum size effect, and the poor conductivity it has. Therefore, the quantum size effect at AgNPs/PAMAM/GCE is clearly, resulting in the conductivity decrease. Another reason may be the higher surface energy of AgNPs, which are easy oxidized, resulting in the poor conductivity.

On the other hand, Electrochemical impedance spectroscopy (EIS) is also used to probe the surface features of the modified electrode (Liao et al., 2010). In the Nyquist plots of the impedance spectra, a semicircle portion observed at higher frequencies would correspond to the electron transfer-limited process, and a linear section at the lower frequencies is attributed to the diffusion limited process. The semicircle diameter corresponds to the electron-transfer resistance (Ret), which can be used to describe the interface properties of the electrode. By using $[Fe(CN)_6]^{3-/4-}$ as the electrochemical probe, the Nyquist plots of different electrodes are shown in Fig. 2B. The impedance spectra of bare GCE (curve a) consisted of a small semicircle (Ret: 68 Ω) with an almost straight tail line, which was the characteristic of a diffusion limiting step of electrochemical process. When the GC electrode was modified with PAMAM, the Ret decreased to 46 Ω (curve b), suggesting that the PAMAM enhanced the conductivity of the modified electrode. However, when AgNPs were electrodeposited on the PAMAM/GC electrode, the diameter of the high frequency semicircle was significantly increased to about 83 Ω (curve c), illustrating that the conductivity of the modified electrode decreased obviously. The result is in agreement with the CV experiment in Fig. 2A.

Fig. 2

In addition, we calculated the average electroactive surface areas of bare GCE and PAMAM/GCE from Fig. S1. The latter (0.118 cm^2) was 1.47 times larger than the former (0.08 cm^2), further proving the PAMAM could provide a large number of active site to load AgNPs.

3.2. Electrochemical response of $O_2\bullet^-$ at AgNPs/PAMAM/GCE

Fig. 3 shows the cyclic voltammograms of different electrodes in the absence (curve a) and presence (curve b) of 1 mM $O_2\bullet^-$ in N_2-saturated 0.2 M PBS solution.

Obviously, current responses in each curve b increase a lot than curve a, suggesting that $O_2•^-$ can produce electrochemical responses in the four different electrodes. It is noticeable that the peak current of $O_2•^-$ at the AgNPs/GCE and AgNPs/PAMAM/GCE (curve b of Fig. 3B and D) intensively enhance than that of bare GCE and PAMAM/GCE (curve b of Fig. 3A and C), revealing that AgNPs have the excellent catalytic activity for the reduction of $O_2•^-$. Meanwhile, the current in curve b of Fig. 3D is the largest among the four pictures, showing AgNPs/PAMAM/GCE is a good sensing platform for detection of $O_2•^-$.

Fig. 3

3.3. Performance of the superoxide anion radical sensor

3.3.1. Optimization of experimental variables

In order to obtain an efficient sensor for detection $O_2•^-$, the analytical conditions, such as the PAMAM concentration, AgNPs electrodeposition time, AgNPs electrodeposition potential and $AgNO_3$ concentration, were optimized by the prepared $O_2•^-$ sensor as shown in Fig. S2. The experiment results showed that the AgNPs/PAMAM/GCE has the best response current for $O_2•^-$ at the following conditions: 7 μL PAMAM (0.5 mg/mL), 180 s electrodeposition time, 0 V electrodeposition potential and 1.0 mM $AgNO_3$ concentration.

3.3.2. Calibration curve of $O_2•^-$ on AgNPs/PAMAM/GCE

Quantitative measurement of $O_2•^-$ concentration was analyzed by linear sweep voltammetry (LSV). Under the optimal experimental conditions, the LSV responses of $O_2•^-$ at AgNPs/PAMAM/GCE were shown in Fig. 4. The current responses of the sensor increased along with $O_2•^-$ concentrations and the relevant linear range for the detection of $O_2•^-$ contained two segments: the response to logarithm of the $O_2•^-$ concentration showed linear range from 7.600×10^{-13}～7.370×10^{-7} mol/L (Fig. 4B), and the linear regression equation was $I_p(\mu A) = 0.3728 \lg [O_2•^-] + 11.22$ with a correlation coefficient of 0.9959. Another linear relationship could be established between the peak current and the concentration of $O_2•^-$ in the range from1.690×10^{-6}～9.180×10^{-5} mol/L (Fig. 4D), and the linear regression equation was $I_p(\mu A) = 0.0179 [O_2•^-](\mu M) + 8.044$ with a correlation coefficient of 0.9988. The detection limit of as-

prepared electrochemical sensor was 2.530×10^{-13} mol/L, at the ratio of signal to noise of 3, which is the lowest in the literatures at present. Of course, the result should be attributed to the amounts of AgNPs loaded on the PAMAM.

A comparison of linear range and detection limit for other $O_2•^-$ sensors reported in literatures is summarized in Table S1. We found that the performance of our proposed sensor provides higher sensitivity and wider linear range than other non-enzymatic $O_2•^-$ biosensors or even far superior to some enzyme biosensors (Wang et al., 2017; Wang et al., 2012).

Fig. 4

3.3.3. Interference immunity, reproducibility and stability of the $O_2•^-$ sensor

Since there are a variety of interferences coexisting in biological samples, it is necessary to perform the anti-interference experiment. Fig. 5 showed the current responses of the AgNPs/PAMAM/GCE with the successive addition of 0.1 mM DA, UA, NO_3^-, NO_2^-, AA, $ONOO^-$, H_2O_2 and $O_2•^-$ in N_2-saturated 0.2 M PBS (pH 7.0) solution at an applied potential -0.5 V. Compared to the remarkable current response of 0.1 mM $O_2•^-$, nearly no currents were observed in DA, UA, NO_3^-, while NO_2^-, AA, $ONOO^-$ were only 4.5%, 9.3%, 5.6% of 0.1 mM $O_2•^-$ current response. But the current response of H_2O_2 was about 17.5% of 0.1 mM $O_2•^-$ cathodic current. As well known, the superoxide ($O_2•^-$) and hydrogen peroxide (H_2O_2) are the two primary products of the ROS, and the detection of ROS released from living cells are generally including $O_2•^-$ and H_2O_2 together. Thus, although H_2O_2 has larger current response, it does not affect the detection of $O_2•^-$, demonstrating that the constructed sensor has good selectivity for monitoring of $O_2•^-$ in biological samples.

Fig. 5

The fabrication reproducibility for five modified electrodes was estimated by comparing the responses of 1 mM $O_2•^-$. As shown in Fig. S3A, the relative standard deviation (RSD) was 3.3%, suggesting the good reproducibility and precision. Moreover, as shown in Fig. S3B, it could retail 93.8% of the original value after 50

segments continuous CV scanning of AgNPs/PAMAM/GCE in the N_2-saturated 0.2 M PBS (pH=7).

Our results further illustrate the reliability of AgNPs/PAMAM modified electrode for determination of $O_2•^-$ since its wide linear range, low detection limit, good anti-interference property and high sensitivity.

3.4. Investigation of the kinetic process of $O_2•^-$ release from living cells

As well known, $O_2•^-$ plays important roles in many biological processes, and it is very important to investigate the kinetic process and quantitative detection $O_2•^-$ release from living cells. Here, rat adrenal medulla pheochromocytoma cell (PC12) was chosen as the model cancer cell, and zymosan was employed as the stimulant agent to induce $O_2•^-$ generation from cancer cells. Firstly, we explored the amperometric current responses in different conditions with AgNPs/PAMAM/GC electrode under an applied potential of -0.5 V. As shown in Fig. 6A, we found that the current of PC12 cell (curve b) was higher than curve a, illustrating the PC12 cells could release ROS constantly and could be detected sensitively by our constructed electrode. When 1.0 μg/mL zymosan was added in PC12 cells at 80 s as shown in curve c, the current increased sharply to a peak value and then decreased gradually, suggesting that ROS was generated rapidly when stimulation by zymosan. When zymosan was added at 130 s again, a similar response was also observed. In order to verify whether the increased current signal was caused by the $O_2•^-$ produced from the stimulated cells, 300 U/mL SOD (a well known selective scavenger of $O_2•^-$) was added to the PC12 cells in advance. In curve d, one can see that the current signal did not change much by zymosan stimulation at 80 s, suggesting that the appearing current was mainly contributed to the release of $O_2•^-$ from the cells.

Secondly, the effect of zymosan dose on the amount of $O_2•^-$ released from PC12 cells was also studied. As shown in Fig. 6B, the currents were increased obviously with the improving concentrations of the stimulated zymosan range from 0.17 to 3.3 μg/mL, respectively, demonstrating the $O_2•^-$ diffused from the cells rapidly with stimulation of a high concentration of zymosan. Meanwhile, the current increases were roughly proportional to the amount of zymosan, showing a zymosan dose-dependent trend.

Furthermore, Fig. 6C showed the amperometric responses of 0.1 μg/mL zymosan stimulating PC12 cells in the absence (curve a) and presence SOD (curve b). In such small dose of zymosan stimulated, a stepwise increase of current responses were observed in curve a. Whereas the presence of SOD in PC12 cells could limit the current increase as shown in curve b, proving SOD could scavenge $O_2•^-$ effectively.

It's worth noting that when added zymosan arrived to a huge concentration (50 μg/mL), an interesting phenomenon could be seen in Fig. 6D. First, a significant current response was observed upon the first stimulus at 80 s (curve a). Then, the next current response decreased obviously as the second injection of zymosan at 130 s again, demonstrating that a large amount of $O_2•^-$, generated in the cells by such heavy dose, could damage cells seriously. This result can be also confirmed by the bright-field microscope images of PC12 cells in stimulated with zymosan conditions (Fig. S4E). However, if 300 U/mL SOD was added to the PC12 cells in advance, as shown in curve b, the current response increased some even though in such big stimulus dose. In addition, the current response for the second stimulus was basically unchanged compared with the first stimulus, which was agreed with the curve b of Fig. 6C. The above experiments proved a significant result that SOD plays an important role in biological systems, that is, it could maintain the $O_2•^-$ concentration at a normal range.

Fig. 6

As well known, superoxide anion is formed in all living organisms and may act as a signaling agent, a harmless intermediate, or a toxic species depending upon its biological context. It could perform the dismutation reaction spontaneously and decompose to H_2O_2 and O_2 quickly in aqueous solution as shown in Eq. (1) (Liu et al., 2017a). Numerous studies found that at high levels, superoxide anions play a major role in the damage of proteins, lipids, and DNA, which may initiate carcinogenesis (Li et al., 2017). This is also observed in curve a of Fig.6D, where a large amount of $O_2•^-$, generated in the cells by such heavy dose, could damage cells seriously.

However, we are just beginning to understand the significance of superoxide dismutases (SOD) in biology and pathology with a wealth of information provided in

this field recently. The SOD enzymes are redox-active metalloenzymes that have involved entirely $O_2•^-$ disproportionation for the purpose of lowering superoxide concentrations as shown in Eq. (2) and Eq. (3) (Sheng et al., 2014). Thus, SOD enzymes are the first and most important line of antioxidant enzyme defense systems against ROS and particularly superoxide anion radicals. That is why SOD could maintain the $O_2•^-$ concentration at a normal concentration, which were also observed in our experiments.

$$2O_2•^- + 2H^+ \longrightarrow O_2 + H_2O_2 \quad (1)$$

$$O_2•^- + \text{enzyme}_{ox} \longrightarrow O_2 + \text{enzyme}_{red} \quad (2)$$

$$O_2•^- + 2H^+ + \text{enzyme}_{red} \longrightarrow H_2O_2 + \text{enzyme}_{ox} \quad (3)$$

What's more, Fig. S4 is the bright-field microscope images of PC12 cells in different conditions. It is clear that PC12 cells were fusiform cells before the experiment (Fig. S4A and Fig. S4D). But as PC12 cells were stimulated by successive adding 0.1 μg/mL zymosan as shown in Fig. S4B and Fig. S4C, we found that the number and morphology of living PC12 cells did not change much no matter SOD present or not. Nevertheless, as 50 μg/mL zymosan was added to the PC12 cells as shown in Fig. S4E, the number of PC12 cells significantly decreased, suggesting that the produced endogenous $O_2•^-$ could damage cells seriously. In Fig. S4F, as 300 U/mL SOD was added in advance to the PC12 cells, the number and morphology of living PC12 cells did not change much compared to Fig. S4C. These results were consistent with the electrochemical experiments.

4. Conclusion

In summary, the main feature of this work is to develop a new platform for reliable collection of kinetic information on cellular superoxide anion release. The proposed AgNPs/PAMAM/GCE sensor realized to detect superoxide anion with an ultra wide linear range and a super low detection limit (2.530×10^{-4} nM). Especially, the electrochemical experiment further confirmed that superoxide dismutase (SOD) could maintain the $O_2•^-$ concentration at lower lever in biological environment, which

is of great significance for us to understand the effects of superoxide dismutases (SOD) in biology and pathology. The results presented in this work open a new way for evaluating the metabolic processes of $O_2•^-$ in the biological system, and has the tremendous potential application in clinical diagnostics to assess oxidative stress.

Supporting Information

The calculation average electroactive surface areas and the optimization of experimental variables, the study of reproducibility and stability of the modified electrode, the bright-field microscope images of PC12 cells under different conditions, and the comparison of various $O_2•^-$ sensors.

Conflict of interest

The authors declare no competing financial interest.

Acknowledgments

This work was supported by the National Natural Science Foundation of China (Nos. 21565021, 31460063).

References

An, Y., Jiang, X., Bi, W., Chen, H., Jin, L., Zhang, S., Wang, C., Zhang, W. 2012. Biosensors and Bioelectronics, 32(1), 224-230.

Amatore, C., Arbault, S., Bouton, C., Coffi, K., Drapier, J.C., Ghandour, H., Tong, Y. 2006. Chembiochem, 7(4), 653-61.

Amatore, C., Arbault, S., Guille, M., Lemaitre, F. 2008. Chem. Rev, 108, 2585-2621.

Brand, M.D., Affourtit, C., Esteves, T.C., Green, K., Lambert, A.J., Miwa, S., Pakay, J.L., Parker, N. 2004. Free Radical Biology & Medicine, 37(6), 755-767.

Cui, K., Song, Y., Yao, Y., Huang, Z., Wang, L. 2008. Electrochemistry communications, 10(4), 663-667.

Dai, Z., Liu, S., Bao, J., Ju, H. 2009. Drug discovery today, 6(8), 427-436.

Haseloff, R.F., Ebert, B., Wischnewsky, G.G. 1991. Analytica chimica acta, 243, 221-225.

Hayyan, M., Hashim, M.A., AlNashef, I.M. 2016. Chemical reviews, 116(5), 3029-3085.

Hu, J., Xu, T., Cheng, Y. 2012. Chemical reviews, 112(7), 3856-3891.

Ignatov, S., Shishniashvili, D., Ge, B., Scheller, F.W., Lisdat, F. 2002. Biosensors and Bioelectronics, 17(3), 191-199.

Kaji, H., Inukai, Y., Maiguma, T., Ono, H., Teshima, D., Hiramoto, K., Makino, K. 2009. Journal of clinical pharmacy and therapeutics, 34(2), 197-205.

Kalpana, D., Cho, S., Lee, S., Lee, Y., Misra, R., Renganathan, N. 2009. Journal of Power Sources, 190(2), 587-591.

Kavosi, B., Salimi, A., Hallaj, R., Amani, K. 2014. Biosensors and Bioelectronics, 52, 20-28.

Lang, H., Maldonado, S., Stevenson, K.J., Chandler, B.D. 2004. Journal of the American Chemical Society, 126(40), 12949-12956.
Li, G., Li, X., Wan, J., Zhang, S. 2009. Biosensors and Bioelectronics, 24(11), 3281-3287.
Li, R.Q., Mao, Z.Q., Rong, L., Wu, N., Lei, Q., Zhu, J.Y., Zhuang, L., Zhang, X.Z., Liu, Z.H. 2017. Biosensors & Bioelectronics, 87, 73-80.
Li, S., Zhu, X., Zhang, W., Xie, G., Feng, W. 2012. Applied Surface Science, 258(7), 2802-2807.
Li, X., Liu, X., Wang, W., Li, L., Lu, X. 2014. Biosensors and Bioelectronics, 59, 221-226.
Li, X., Liu, Y., Zheng, L., Dong, M., Xue, Z., Lu, X., Liu, X. 2013. Electrochimica Acta, 113, 170-175.
Liao, Y., Yuan, R., Chai, Y., Zhuo, Y., Yang, X. 2010. Analytical biochemistry, 402(1), 47-53.
Liu, L., Zhao, H., Shi, L., Lan, M., Zhang, H., Yu, C. 2017a. Electrochimica Acta, 227, 69-76.
Liu, Y., Liu, X., Liu, Y., Liu, G., Ding, L., Lu, X. 2017b. Biosensors and Bioelectronics, 90, 39-45.
Ning, D., Zhang, H., Zheng, J. 2014. Journal of Electroanalytical Chemistry, 717, 29-33.
Prasad, S., Gupta, S.C., Tyagi, A.K. 2017. Cancer Lett, 387, 95-105.
Scott, R.W., Wilson, O.M., Oh, S.-K., Kenik, E.A., Crooks, R.M. 2004. Journal of the American Chemical Society, 126(47), 15583-15591.
Sheng, Y., Abreu, I.A., Cabelli, D.E., Maroney, M.J., Miller, A.F., Teixeira, M., Valentine, J.S. 2014. Chem Rev, 114(7), 3854-918.
Tomalia, D.A. 2012. Interview: Nanomedicine, 7(7), 953-956.
Wang, M.-Q., Ye, C., Bao, S.-J., Xu, M.-W., Zhang, Y., Wang, L., Ma, X.-Q., Guo, J., Li, C.-M. 2017. Biosensors and Bioelectronics, 87, 998-1004.
Wang, M.-Q., Ye, C., Bao, S.-J., Zhang, Y., Yu, Y.-N., Xu, M.-w. 2016. Analyst, 141(4), 1279-1285.
Wang, X., Han, M., Bao, J., Tu, W., Dai, Z. 2012. Analytica chimica acta, 717, 61-66.
Wang, X., Zhang, Y., Li, T., Tian, W., Zhang, Q., Cheng, Y. 2013. Langmuir, 29(17), 5262-5270.
Wu, L., Zhang, X., Chen, J. 2014. Journal of Electroanalytical Chemistry, 726, 112-118.
Xie, Z., Huang, J., Xu, X., Jin, Z. 2008. Food Chemistry, 111(2), 370-376.
Zhou, Y., Ding, J., Liang, T., Abdel-Halim, E.S., Jiang, L., Zhu, J.J. 2016. ACS Appl Mater Interfaces, 8(10), 6423-30.
Zhu, X., Liu, T., Zhao, H., Shi, L., Li, X., Lan, M. 2016. Biosens Bioelectron, 79, 449-56.
Zweier, J.L., Flaherty, J.T., Weisfeldt, M.L. 1987. Proceedings of the National Academy of Sciences, 84(5), 1404-1407.

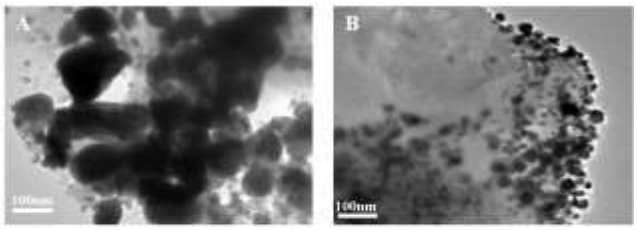
A
B
100nm

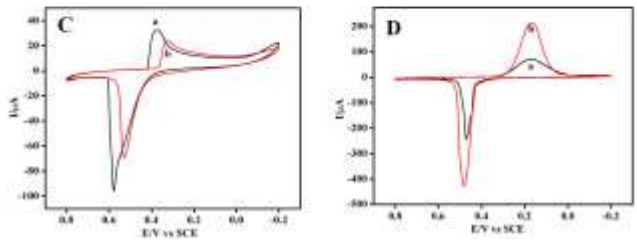
C
D
E/V vs SCE

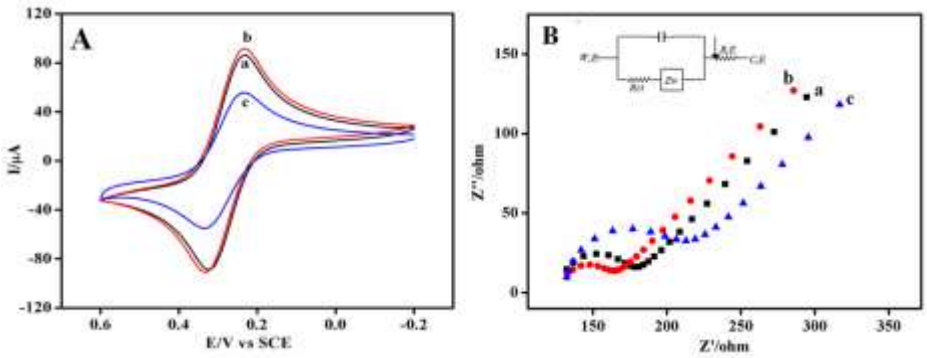
A
B
I/μA
E/V vs SCE
Z''/ohm
Z'/ohm

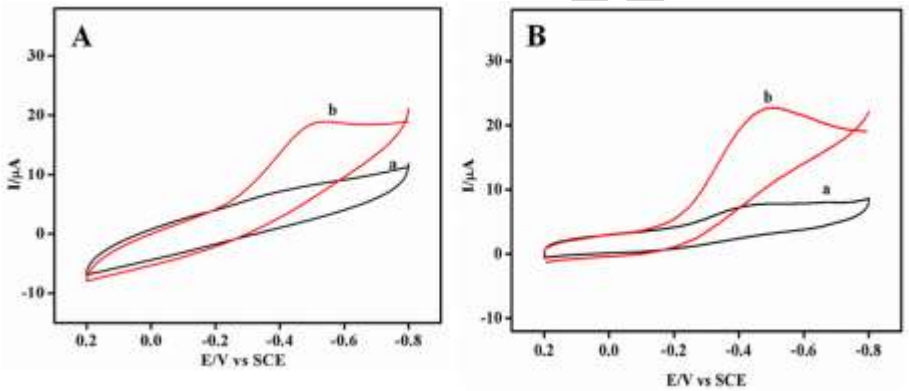
A
B
I/μA
E/V vs SCE

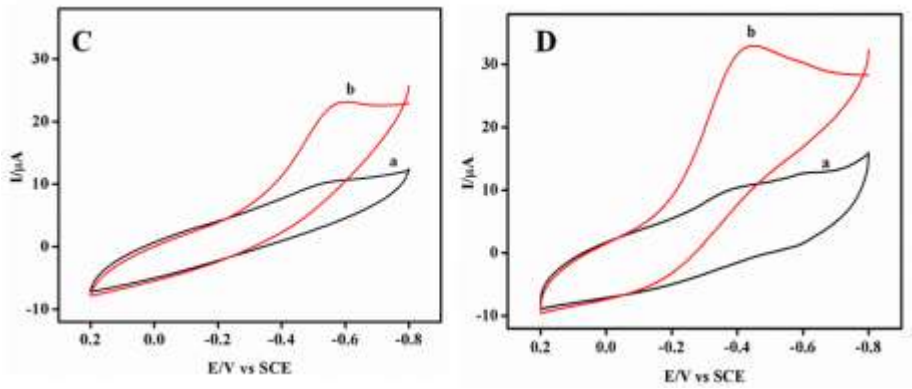
C
D
I/μA
E/V vs SCE

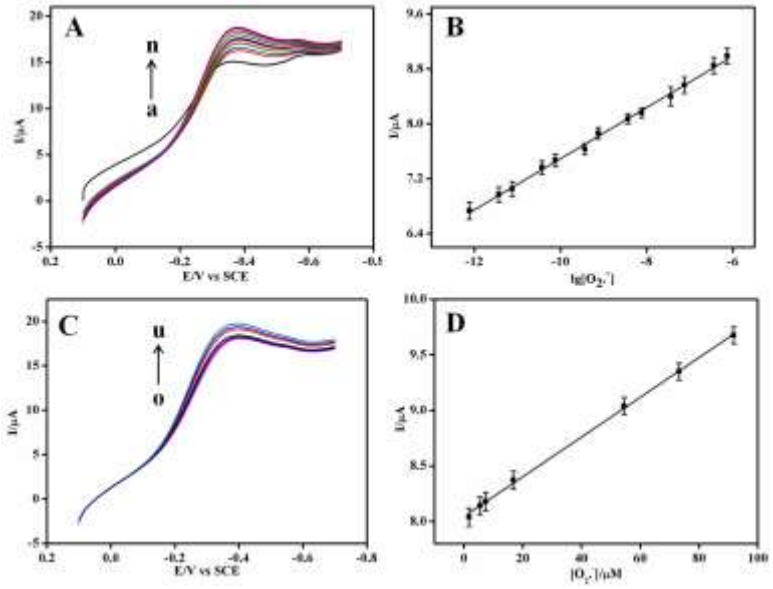
A
n
a
I/μA
E/V vs SCE
B
I/μA
lg[O2·-]
C
u
o
I/μA
E/V vs SCE
D
I/μA
[O2·-]/μM

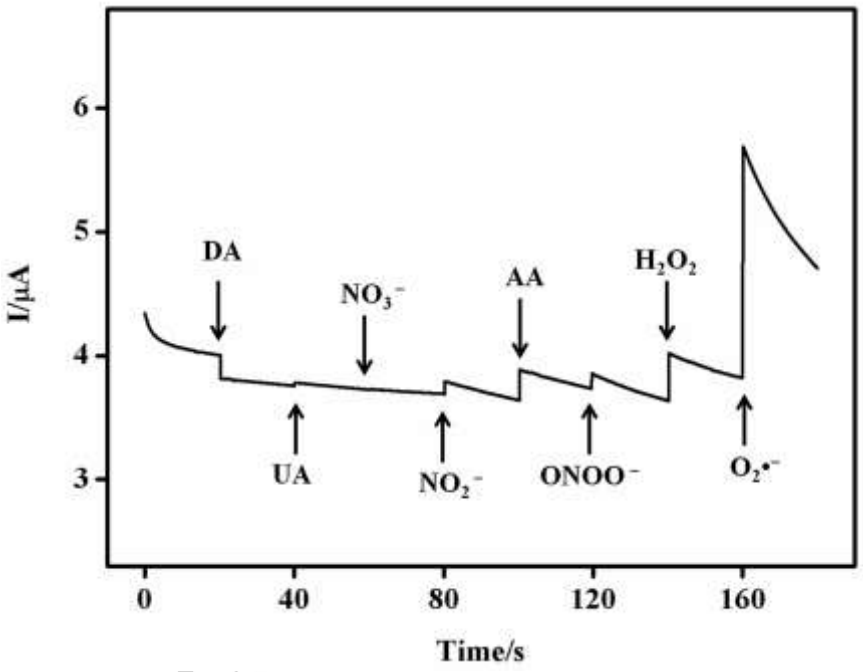
DA
NO3-
AA
H2O2
UA
NO2-
ONOO-
O2•-
I/μA
Time/s

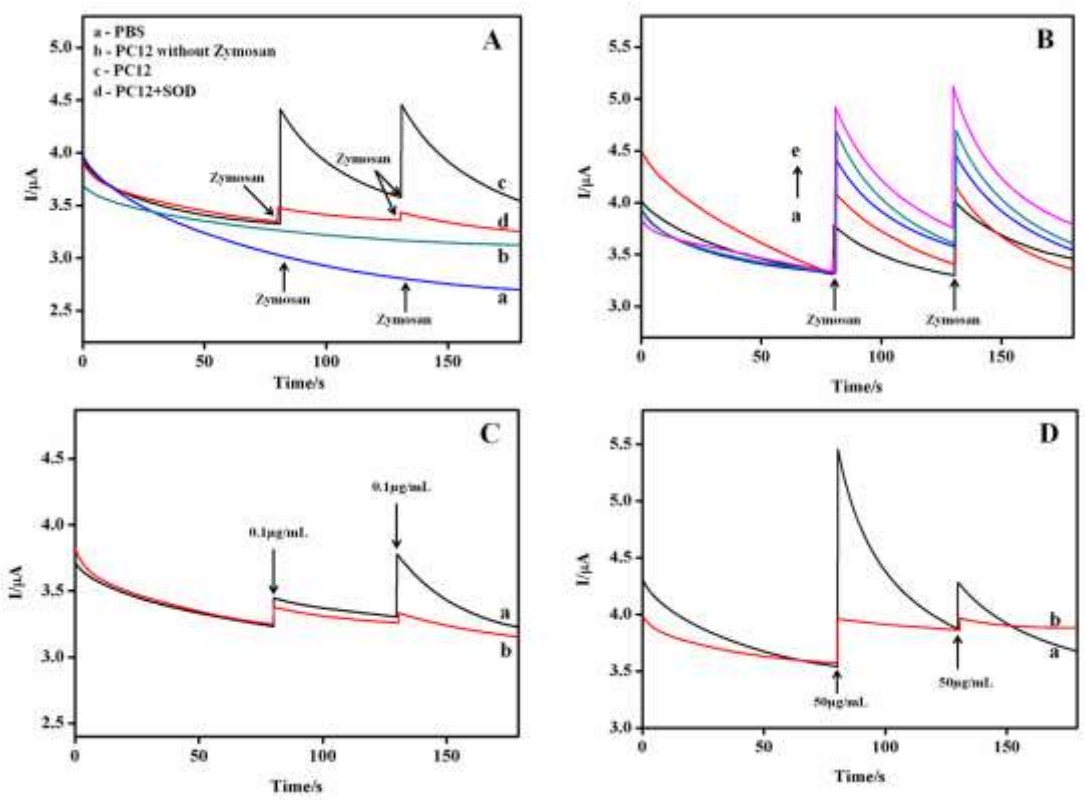

Figure captions

Fig. 1. TEM images of various modified GCE substrates (A) AgNPs/GCE and (B) AgNPs/PAMAM/GCE; (C). Cyclic voltammograms of bare GCE (a) and PAMAM/GCE (b) in the solution of 1.0 mM $AgNO_3$ + 0.1 M KNO_3; (D) Cyclic voltammograms recorded using AgNPs/GCE (a) and AgNPs/PAMAM/GCE (b) in N_2-saturated 0.2 M PBS (pH 7.0), at 50 mV/s.

Fig. 2. (A) Cyclic volatmmograms and (B) EIS of bare GCE (a), PAMAM/GCE (b) and AgNPs/PAMAM/GCE (c) in 5 mM $[Fe(CN)_6]^{3-/4-}$ solution with 0.1 mol/L KNO_3, at 50mV/s.

Fig. 3. CVs of different electrodes in the absence of $O_2\bullet^-$(curve a) and the presence of 1.0 mM $O_2\bullet^-$ (curve b): (A) bare GCE, (B) AgNPs/GCE, (C) PAMAM/GCE, (D) AgNPs/PAMAM/GCE, at 100mV/s.

Fig. 4. (A) LSV curves of AgNPs/PAMAM/GCE in N_2–saturated 0.2 M PBS (pH 7.0) containing various concentrations of $O_2\bullet^-$ (from a to n: 0, 7.6×10^{-13}, 3.71×10^{-12}, 7.62×10^{-12}, 3.69×10^{-11}, 7.57×10^{-11}, 3.67×10^{-10}, 7.52×10^{-10}, 3.64×10^{-9}, 7.66×10^{-9}, 3.62×10^{-8}, 7.42×10^{-8}, 3.59×10^{-7}, 7.37×10^{-7} M) at −0.38 V; (B) The calibration curve between current and $\lg[O_2\bullet^-]$. (C) LSV curves of AgNPs/PAMAM/GCE with successive addition of $O_2\bullet^-$ (from o to u: 1.69×10^{-6}, 5.48×10^{-6}, 7.37×10^{-6}, 1.68×10^{-5}, 5.45×10^{-5}, 7.32×10^{-5}, 9.18×10^{-5} M) to N_2-saturated 0.2 M PBS (pH 7.0) at −0.38 V; (D) The calibration plots illustrating the linear electrode response to $O_2\bullet^-$ addition. Scan rate: 100 mV/s.

Fig. 5. Amperometric i-t responses of AgNPs/PAMAM/GCE upon the successive addition of 0.1 mM DA, UA, NO_3^-, NO_2^-, AA, $ONOO^-$, H_2O_2 and $O_2\bullet^-$ in N_2-saturated 0.2 M PBS (pH 7.0) solution with an applied potential -0.5 V under a stirring condition.

Fig. 6. (A) Time course of the $O_2\bullet^-$ release in different situation: blank PBS upon the successive addition of 1 μg/mL zymosan (a), PC12 cells (b), PC12 cells upon the successive addition of 1 μg/mL zymosan (c), PC12 cells and 300 U/mL SOD upon the stimulation of 1 μg/mL zymosan (d). (B)The amperometric responses of $O_2\bullet^-$ released from PC12 cells induced by 0.17 (a), 0.5 (b), 1.0 (c), 2.5 (d) and 3.3 μg/mL of zymosan (e). (C) and (D) show the amperometric responses of different concentrations of 0.1 μg/mL and 50 μg/mL zymosan stimulating PC12 cells in the absence (curve a) and presence SOD (curve b).

Highlights

1. Fabricated a novel sensor with PAMAM as effective matrix loading on great amount of AgNPs.
2. It displays excellent performance toward $O_2^{\bullet -}$ with a super low detection limit (2.53×10^{-4} nM).
3. It was used for in situ detecting the $O_2^{\bullet -}$ release from living cells with satisfactory results.
4. Study the kinetics process of $O_2^{\bullet -}$ release from living cells for the first time.
5. The experiment found that SOD could maintain the $O_2^{\bullet -}$ concentration at lower lever in biological environment.